Dynamic Stark Spectroscopic Measurements of Microwave Electric Fields Inside the Plasma Near a High-Power Antenna

C. C. Klepper,[1,*,†] R. C. Isler,[1] J. Hillairet,[2] E. H. Martin,[3,1] L. Colas,[2] A. Ekedahl,[2] M. Goniche,[2] J. H. Harris,[1] D. L. Hillis,[1] S. Panayotis,[2] B. Pegourié,[2] Ph. Lotte,[2] G. Colledani,[2] V. Martin,[2] and Tore Supra Lower Hybrid Systems Technical Team

[1]*Oak Ridge National Laboratory, Oak Ridge, Tennessee 37831-6169, USA*
[2]*CEA, IRFM, F-13108 Saint Paul-Lez-Durance, France*
[3]*North Carolina State University, Raleigh, North Carolina 27695, USA*

(Received 31 October 2012; published 21 May 2013)

Fully dynamic Stark effect visible spectroscopy was used for the first time to directly measure the local rf electric field in the boundary plasma near a high-power antenna in high-performance, magnetically confined, fusion energy experiment. The measurement was performed in the superconducting tokamak Tore Supra, in the near field of a 1–3 MW, lower-hybrid, 3.7 GHz wave-launch antenna, and combined with modeling of neutral atom transport to estimate the local rf electric field amplitude (as low as 1–2 kV/cm) and direction in this region. The measurement was then shown to be consistent with the predicted values from a 2D full-wave propagation model. Notably the measurement confirmed that the electric field direction deviates substantially from the direction in which it is launched by the waveguides as it penetrates only a few cm radially inward into the plasma from the waveguides, consistent with the model.

DOI: 10.1103/PhysRevLett.110.215005 PACS numbers: 52.70.Gw, 52.20.Fs, 52.35.Hr, 52.70.Ds

Radio-frequency (rf) waves have long been used to heat plasmas in industrial applications and to provide both heating and current drive in fusion energy research. While the physics mechanisms of the wave heating and current drive processes in the bulk plasma are generally understood, the details of wave launching from the antenna into the plasma involve plasma-material interactions and sheath physics that are difficult to diagnose and model accurately in real geometry. In practice, coupling of rf antennas to hot plasma is thus largely empirical. This approach becomes problematic in large tokamak fusion experiments, where it is necessary to efficiently launch megawatts of power from antennas with sizes ~ 1 m^2. Experiments on tokamaks such as Tore Supra [1] show that significant fractions of the launched rf power return to the antenna structure in concentrated (few cm) ''hot-spots'' with fluxes of $\sim$1–20 MW/m^2 [1]. These high heat-fluxes can burn through thin-walled, water-cooled antenna components and cause coolant leaks, posing serious operational risks, especially for a *D-T*, neutron producing device such as ITER [2]. *In situ* measurements of rf wave fields in the near-field region of the antenna are needed to validate coupling models and guide optimization of antenna design and operation. Although detailed measurements with material probes, primarily driven to verify basic wave-launch and propagation physics, have been performed (see, e.g., Refs. [3–5]), concerns with probe perturbations and survival have limited such studies to relatively low density and temperature plasmas, mostly confined in linear magnetic confinement devices.

In this Letter, we present the results of nonperturbing, spectroscopic measurements of rf wave fields within the plasma-antenna interaction region of a high-power (>1 MW) antenna, operating in edge of a large fusion energy plasma device. It was accomplished by measuring deuterium Balmer-series spectral line profiles (influenced by the dynamic Stark effect) and fitting these to a time-dependent, Stark effect, spectral profile model. The results were then combined with local plasma characterization and neutral transport modeling to localize the emission region. Information has been obtained about both the magnitude and the direction of the local rf electric fields and validated by comparison to two dimensions, full-wave-propagation modeling. The experiments presented here were carried out on the Tore Supra superconducting, long-pulse (25 s to nearly 6 min) tokamak, whose non-inductive current drive operation is achieved primarily through the coupling of lower hybrid (LH) waves. These are directionally launched by two, large (~ 60 cm $\times$ 60 cm), specially configured antennas each rated for operation of up to 4 MW at 3.7 GHz.

Figure 1 shows the structural configuration of the observed antenna (the ''*C*3 Launcher'' [6]). Its plasma-facing side comprises a grill structure formed by the two-dimensionally stacked ends of phased waveguides and two lateral protection limiter (LPL) structures. The latter are actively cooled and designed to protect the grill from direct exposure to the boundary layer plasma [7]. The phased array is configured such that the rf wave is initially launched with E_{rf} parallel to the confining (nearly toroidal) magnetic field B_t throughout the aperture of the antenna.

The spectroscopic sightline was provided by means of an *endoscope* at an outer mid-plane location near the outer wall opposite the antenna, recessed in its access port to

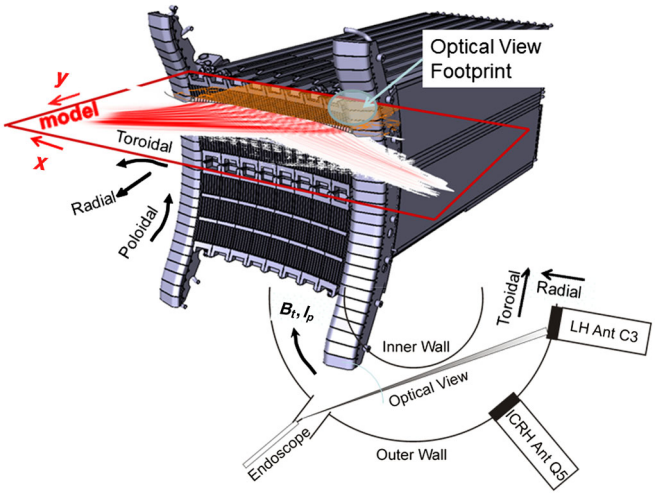

FIG. 1 (color online). Structure of the wave-launch side of the C3 LH launcher. Insets show a typical, 2D $|E_{rf}|$ map obtained through full-wave computation; the pattern is asymmetric, which results ultimately in net current being driven in the plasma. The spectroscopic sightline from the recessed end of the endoscope and the footprint it casts onto the left limiting structure are also illustrated.

protect from direct exposure to radiated heat during long-pulse, high-power tokamak plasma operation. This limited optical access through the ~1 m-thick cryostat containing the B_t coils, restricted the optical view to a region around the left-hand side (from the launcher's perspective) LPL and casting a large ~0.20 m diam, nearly circular footprint on the antenna, about 4 m from the endoscope's first mirror.

Figure 2 shows measured and modeled spectral profiles of the D_β spectral line recorded over two different plasma discharge intervals, each having a different LH power level, constant over several seconds. The discrete, experimental measurement points represent data integrated over exposure times of 0.5 s under steady state conditions. Uncertainties based on counting statistics are about 2% at the peak of the signals. Each of the measured profiles is observed to mainly consist of three groups of broadened lines. The physical processes that produce the broadening have not been identified.

The experimental data are modeled from solutions to the time-dependent Schrödinger equation including perturbations from the spin-orbit interaction, a static magnetic field (B_t), and a dynamic electric field E_{LH} at the LH frequency [8–10]. Although the computation developed for this work follows the dynamic Stark effect formalism of Ref. [8], the model had to be expanded and generalized to include the Tesla-level magnetic fields of the tokamak and arbitrary angles between rf electric field, static magnetic field and sightline. Because the physics of the broadening mechanisms are not well understood, the model assumes a modified Lorentz profile for each transition comprising the profile. The wings of the lines are sometimes not well described by this assumption, but it does not severely influence the interpretation of the field strength and its

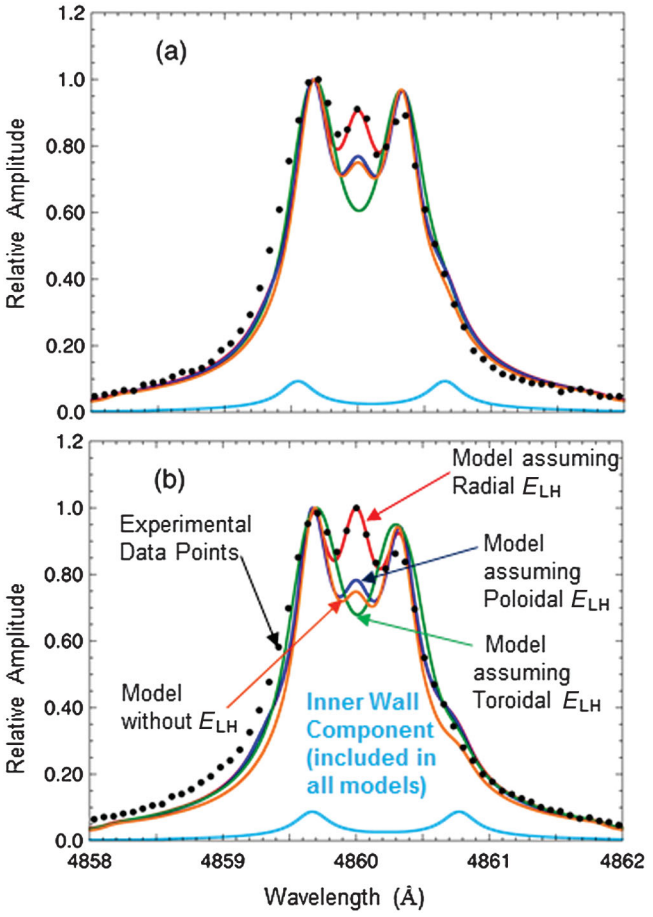

FIG. 2 (color). D_β spectral profiles for Tore Supra Shot 47 915. (a) 1.92 MW LH power. Black circles are measured data. Red, dark blue, and green curves, respectively, represent models for a 1.5 kV/cm dynamic electric field in the radial, poloidal, and toroidal directions. Orange is the $E_{LH} = 0$ model, consistent with the broadened Zeeman profile expected from the outboard (low-B_t) boundary, where the sightline is at 54° with B_t, but the central (π) component is partly suppressed by the endoscope's mirror operating at a grazing angle. Light blue is the assumed inner-edge contribution. (b) Same as (a) except LH power is 3.37 MW and model $|E_{LH}| = 2.0$ kV/cm, clearly increasing with power.

direction, which are inferred from the fits to the central part of the profile.

It was also quite clear in many discharges, during periods when the antenna was not operating, that the sightline passes close enough to the inner wall to detect a significant contribution from the high magnetic-field side (inner boundary) of the plasma. This component is distinguished by a comparatively large Zeeman splitting and a wavelength shift when compared to the component near the antenna. The component near the antenna becomes dominant when it is operating; however a minor inner-boundary contribution is still present and is apparently responsible for the asymmetries of the data observed in Fig. 2.

The four modelled profile traces shown in each of the two LH power cases of Fig. 2 are best fits to the

experimental data but for different assumptions regarding the direction of the rf (dynamic) electric field. These modeled profiles are clearly distinguished from the amplitude of the central feature. They show that *radially directed* electric fields of magnitude 1.5 and 2.0 kV/cm (for the 1.92 MW and 3.37 MW cases, correspondingly) produce significant amplitudes for the central component, just as observed in the data. Profiles calculated assuming zero rf field or fields in the *poloidal* or *parallel* direction do not match the data. The relatively weak, inner-boundary component, which is common to all three models, is also shown in each frame of the figure. Although a more precise determination of the rf field's polarization is precluded by the present data, the ability to match the peak feature only with a radially directed E_{rf}, leads us to conclude that this is the predominant orientation in the observed region.

This finding is surprising at first glance, because the LH antenna is designed to launch waves with $E_{\mathrm{rf}} \parallel B_t$. The end of each of the grill's waveguides is oriented such that the E_{rf} is launched toroidally and the grill surface is profiled to conform to the local field-line shape, including its ripple due to the discrete number of B_t coils.

To determine the direction of E_{rf} inside the measurement volume of the plasma in realistic geometry, we combine full-wave modeling of LH-wave propagation with Monte Carlo modeling of the transport, molecular dissociation and excitation of the D_β-emitting neutrals in the low-temperature, low-density plasma in front of the antenna.

The full-wave computation, also illustrated in Fig. 1, used the finite-element COMSOL$^{\mathrm{TM}}$ Multi-Physics software package to solve the wave equations in the launcher and in the plasma-antenna interaction region, similarly to Ref. [11]. The exact launcher geometry is taken from the computer-aided design (CAD) model, together with its LPLs. The plasma is modeled by a cold-plasma dielectric-tensor with a realistic magnetic field configuration. Since the model is numerically solved, any electron density and temperature (n_e, T_e) radial profile can be entered. In this work, a bilinear profile, conformal to the magnetic field-line shape, has been used for n_e. The shown model is for a SOL n_e decay-length $\lambda_{ne} = 2$ cm. The model is sensitive to λ_{ne} and its value was determined from fitting Langmuir probe data for similar discharges. Artificial collisions are added at the inner part of the simulation to damp the LH wave.

Figure 3 shows a more detailed graphical output of the model, limited to a spatial region near the observation location at the launcher, and including both the strength (absolute magnitude) and the direction (polarization, here normalized) of E_{LH}. These are mapped on a 2D, toroidal cross section, for the antenna geometry and for typical rf power and plasma conditions of the described experiments and under steady-state conditions. The key thing to note here is that the polarizations of E_{LH} strongly deviate from the original $\parallel B_t$ direction while only a short distance from

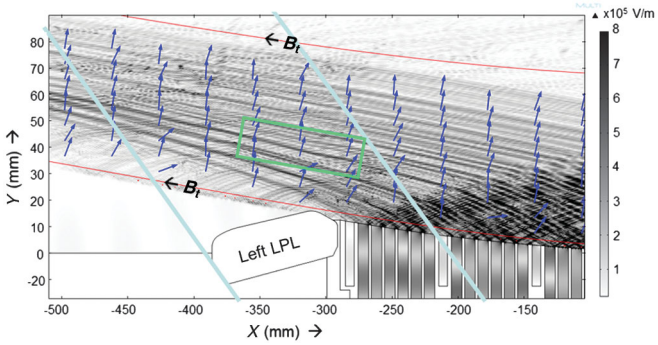

FIG. 3 (color). Detail of the LH wave model. Gray scale map represents $|E_{\mathrm{LH}}|$ maxima (scale 0–8 $\times 10^5$ V/m), dark-blue vectors are normalized directions for E_{LH} and the green box is a simplified illustration of the approximate region of significant D_β emission (from EIRENE). The red, solid lines indicate the shape of the local ripple-corrected, magnetic field lines. Light-blue lines outline the edges of the broad sightline.

the mouth of the antenna. In fact, in the region in front of the LPL the orientation is largely $\perp B_t$.

The physical process that changes the orientation of E_{LH} from $\parallel$ to nearly $\perp$ can be better understood with the following calculation. For the sake of simplicity the LH wave propagation at angular frequency ω_0 is studied in 2D slab geometry, where (x, y) denote respectively the parallel and radial coordinates and $y = 0$ at the grill mouth. Figure 3 exhibits small-scale near-field structures with a toroidal extension well below the LH wavelength in vacuum (~ 8 cm at the rf frequency of 3.7 GHz). Therefore, the propagation of the LH parallel electric field $E_{\parallel\mathrm{LH}}$ is well approximated by the electrostatic slow wave (SW) equation ([12] p. 222)

$$P(y, \omega_0)\Delta_\perp E_{\parallel\mathrm{LH}} + S(y, \omega_0)\Delta_\parallel E_{\parallel\mathrm{LH}} = 0, \qquad (1)$$

where Δ is the Laplace operator. In the tenuous plasma surrounding the launcher the cold-plasma Stix parameters $P(y, \omega_0)$ and $S(y, \omega_0)$ can be defined as a function of the local electron density $n(y)$ according to [[13] p. 7, Eqs. (19) and (22), [12] p. 224]

$$\begin{aligned} &P(y, \omega_0) = 1 - n(y)/n_c(\omega_0); \\ &S(y, \omega_0) \sim 1 \text{ near LH launcher.} \end{aligned} \qquad (2)$$

At 3.7 GHz the critical density is $n_c(\omega_0) \sim 1.7 \times 10^{17}$ m^{-3}. For the measured density profiles, $P < 0$ in the region probed by the diagnostic so that the electrostatic SW is propagative. From Eq. (1) the LH near field is then organized in two lobes of the form

$$\begin{aligned} E_{\parallel\mathrm{LH}}(x, y) = E^+\left(x + \int_0^y \left|\frac{P(y', \omega_0)}{S(y', \omega_0)}\right|^{1/2} dy'\right) \\ + E^-\left(x - \int_0^y \left|\frac{P(y', \omega_0)}{S(y', \omega_0)}\right|^{1/2} dy'\right). \end{aligned} \qquad (3)$$

The positive lobe E^+ propagates to the left of Fig. 3 and provides the main contribution to E_{LH} in the region

probed by the diagnostic. In this lobe the electric field polarisation in the electrostatic approximation is expressed as ([12] p. 229)

$$\frac{E_{\perp \mathrm{LH}}}{E_{\parallel \mathrm{LH}}} = -\left|\frac{P}{S}\right|^{1/2}. \quad (4)$$

As the local density increases towards the main plasma, $|P/S|$ grows and the lobes, initially perpendicular to B_t, progressively bend towards the parallel direction. At the same time E_{LH} progressively shifts in direction to become nearly perpendicular to B_t.

The next question is whether it is possible to define the spatial region, which contributes most to the light collected near the antenna, and whether the direction of E_{LH} can be more precisely predicted for that region. For this, a neutral particle transport simulation was performed for the deuterium recycling at the antenna's plasma-facing components (PFC), including molecular dissociation processes, which can dominate the D_β emission near PFCs.

The green rectangle overlaid onto the 2D field map of Fig. 3 represents the estimated region of significant D_β emission, based on a simulation using the 3D Monte Carlo code EIRENE [14]. Simulations are performed in a cylindrical geometry of radius equal to the curvature of the antenna surface (~ 73 cm); n_e, T_e profiles are taken from probe measurements [Fig. 4(a)] and are representative of the discharges discussed here. An ion flux normalized to 1A is launched from the confined plasma and recycles on the surface of the cylinder. (Carbon surface is assumed; this governs the proportion of molecules and atoms in the recycling flux; typical values are $0.4 * D_2 + 0.2 * D$, see, e.g., Ref. [15]). The ionization source is calculated by taking into account the different possibilities of molecular dissociation, ionization, the successive generations of charge-exchange atoms and the reflection of neutrals on the wall. Added utility in EIRENE allows the computation of the emission probability for a specific Balmer-series line, such as D_β and this result is displayed in Fig. 4(b).

Thus the rectangle in Fig. 3 illustrates the likely region, within the broad sightline, contributing most of the measured D_β emission. Its height represents approximately the width of the broad peak in the curve of Fig. 4(b), which in the 1D EIRENE simulation is a zone of constant width and parallel to antenna. Its width is roughly defined by the assumption that most of the neutrals originate from plasma neutralization and recycling at the LPL with a maximum at the point of closest approach to the plasma. This interaction can be assumed to decrease asymmetrically with toroidal distance from this point, with a decay length $\sim \times 10$ shorter in the private side region (between the two LPLs) than on the side of the observed LPL that faces away from the antenna grill [16].

It is clearly seen that all E_{LH} vectors within this region are nearly perpendicular to the B_t lines (Fig. 3). This is consistent with the result of fitting the data to the spectral model, in which a viable solution could only be found when E_{LH} was taken to be $\perp B_t$ and in the radial direction (i.e., also $\perp$ to the mouth of the antenna). Furthermore, using the scale on the right of the figure, it is seen that $|E_{\mathrm{LH}}|$ averages to about 3 kV/cm, which is within a factor of 2 of the value for the best fit of the data.

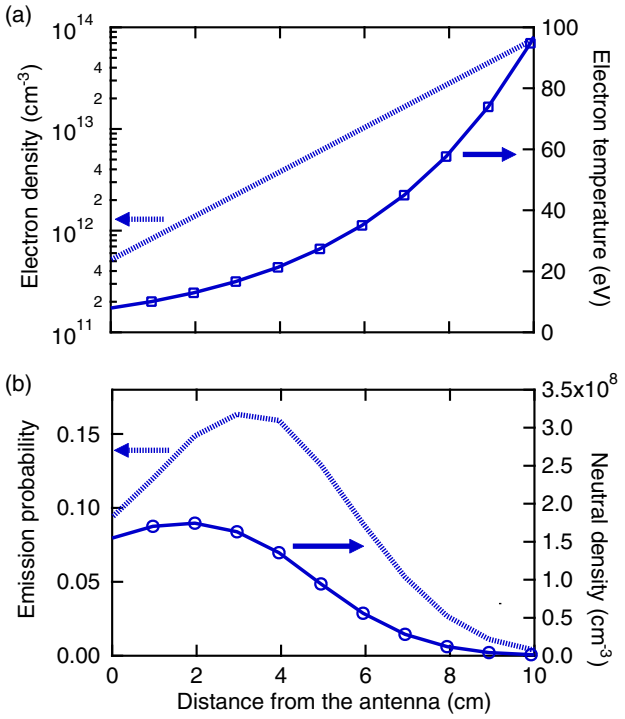

FIG. 4 (color online). Neutral transport modeling: (Top) Input n_e, T_e profiles are from Langmuir probe measurements from LH injection experiments, similar to that of shot 47 915. (Bottom) Radial probability profile for D_β emission computed from the output neutral density (also shown) and ionization profiles, using branching-ratio data.

In conclusion, the combination of dynamic Stark-effect, visible-range spectroscopic measurements and neutral atom transport computation (for measurement localization of the long-range, passive, optical detection) yields measurements of the local rf electric field amplitude (as low as 1–2 kV/cm) and direction in the near-field antenna-plasma interaction region of a magnetically confined plasma consistent with modeling of 2D full-wave propagation. The first application of this new technique to a lower-hybrid launcher in Tore Supra already provides experimental verification that the electric field direction deviates substantially from the direction in which it was launched by the waveguides as it penetrates only a few cm radially inward into the plasma, consistent with both analytical and numerical models. Further studies using more refined instruments to cover larger portions of the antenna interaction region would yield a more comprehensive picture of the wave launching process and could also be applied to other heating schemes such as ion cyclotron

resonance-frequency heating (ICRH). The improved understanding that emerges from such studies should contribute significantly to the development of more effective antenna designs and operational strategies for launching the very high rf heating powers needed for reactor-scale fusion confinement devices such as ITER, while keeping antenna surface heating of antennas and other plasma-facing components to an acceptable level.

This work was supported in part by the U.S. DOE under Contract No. DE-AC05-00OR22725 with UT-Battelle, LLC., and in part by the European Communities under the contract of Association between EURATOM and CEA and within the framework of the European Fusion Development Agreement. The views and opinions expressed herein do not necessarily reflect those of the European Commission.

*To whom all correspondence should be addressed. kleppercc@ornl.gov, kleppercc@ieee.org

†Present address: CEA, IRFM, SCCP/Bat-513, F-13108 Saint Paul-lez-Durance, France.

[1] Tore Supra Special Issue, Fusion Sci. Technol. **56**, 1079 (2009).

[2] R. Aymar, P. Barabaschi, and Y. Shimomura, Plasma Phys. Controlled Fusion **44**, 519 (2002).

[3] R. L. Stenzel and W. Gekelman, Phys. Rev. A **11**, 2057 (1975).

[4] S. Rosenberg and W. Gekelman, J. Geophys. Res. **106**, 28867 (2001).

[5] S. Bernabei, M. A. Heald, W. M. Hooke, and F. J. Paoloni, Phys. Rev. Lett. **34**, 866 (1975).

[6] Ph. Bibet *et al.*, Fusion Eng. Des. **51–52**, 741 (2000).

[7] G. Agarici *et al.*, Fusion Eng. Des. **49–50**, 145 (2000).

[8] W. Hicks, R. Hess, and W. Cooper, Phys. Rev. A **5**, 490 (1972).

[9] S. Hirsch and G. Himmel, Z. Phys. D **16**, 35 (1990).

[10] O. Peyrusse, Phys. Scr. **56**, 371 (1997).

[11] S. Shiraiwa, O. Meneghini, R. Parker, P. Bonoli, M. Garrett, M. C. Kaufman, J. C. Wright, and S. Wukitch, Phys. Plasmas **17**, 056119 (2010).

[12] M. Brambilla, *Kinetic Theory of Plasma Waves* (Oxford Science Pub., New York, 1998).

[13] T. H. Stix, *Waves in Plasmas* (AIP, New York, 1992).

[14] D. Reiter, M. Baelmans, and P. Börner, Fusion Sci. Technol. **47**, 172 (2005).

[15] W. Eckstein, *Atomic and Plasma-Material Interaction, Data for Fusion, Supplement to Nuclear Fusion* Vol. 1 (IAEA, Vienna, 1991), p. 17.

[16] M. Preynas *et al.*, Nucl. Fusion **51**, 023001 (2011).